Photoionization and electron-impact ionization of Kr^{5+}

M. Lu, M. F. Gharaibeh, G. Alna'washi, and R. A. Phaneuf
Department of Physics, MS 220, University of Nevada, Reno, Nevada 89557-0058, USA

A. L. D. Kilcoyne, E. Levenson, and A. S. Schlachter
Advanced Light Source, Lawrence Berkeley National Laboratory, MS 7-100, Berkeley, California 94720-8225, USA

A. Müller, S. Schippers, and J. Jacobi
Institut für Atom-und Molekülphysik, Justus-Liebig-Universität, 35392 Giessen, Germany

S. W. J. Scully
Depatment of Physics and Astronomy, Queen's University, Belfast BT7 1NN, Northern Ireland

C. Cisneros
Centro de Ciencias Fisicas, Universidad Nacional Autónoma de México, Apartado Postal 6-96, Cuernavaca 62131, Mexico
(Received 11 May 2006; published 6 July 2006)

Absolute photoionization cross sections for Kr^{5+} were measured in the photon energy range 74–175 eV using synchrotron radiation. For comparison, a detailed energy scan of the electron-impact ionization cross section was made in the same energy range and normalized to previously published absolute measurements. The Flexible Atomic Code and Cowan atomic structure code were used to calculate energy levels, excitation energies, and oscillator strengths for $3d \rightarrow np$, $3d \rightarrow nf$, and $4s \rightarrow np$ autoionizing transitions from the ground and metastable states. Within the experimental uncertainty, oscillator strengths determined from the photoionization measurements are in agreement with both calculations. Excitation-autoionization and resonant excitation-double-autoionization features are evident in the electron-impact ionization cross section.

DOI: 10.1103/PhysRevA.74.012703 PACS number(s): 32.80.Fb, 34.80.Dp, 32.80.Dz, 32.70.Cs

I. INTRODUCTION

Electron-impact ionization and photoionization of ions are important atomic processes in laboratory and astrophysical plasmas such as those encountered in controlled thermonuclear fusion research. An important element in those experiments is krypton, which is introduced as a diagnostic impurity for the central core, as a source of electrons for studies of the edge plasma, and as a radiation "coolant" for diverters [1–5]. Highly ionized krypton ions are dominant in the core plasma, whereas ions in moderate to low charge states are abundant in the edge plasma. As a result, theoretical and experimental data on electron-impact and photon-impact excitation and ionization of the krypton atom and its ions are needed for the modeling of such plasmas.

Electron-impact excitation and ionization of the neutral krypton atom and its ions have been studied extensively over the last few decades, both experimentally and theoretically. On the experimental side, the electron-impact ionization cross section for the neutral krypton atom has been measured by several groups [6–8]. Ionization cross sections were measured by Tinschert *et al.* for Kr^{+}, Kr^{2+}, and Kr^{3+} [9] and by Bannister *et al.* for Kr^{4+}, Kr^{5+}, Kr^{7+}, [10] and Kr^{8+} [11]. Oualim *et al.* [12] reported ionization cross-section measurements for Kr^{10+} and Kr^{11+}, and measurements for Kr^{12+} through Kr^{18+} have been reported recently by Khouilid *et al.* [13]. On the theoretical side, Gorczyca *et al.* [14] carried out configuration-average distorted-wave calculations for the electron-impact ionization of Kr^{4+}, Kr^{5+}, Kr^{6+}, and Kr^{7+}, while also studying term-dependence and resonance-excitation effects within the distorted-wave and close-coupling approximations for Kr^{6+} and Kr^{7+}. Mitnik *et al.* [15] carried out fully relativistic distorted-wave calculation for the ionization of Kr^{6+}. Ionization cross sections for Kr^{10+} and Kr^{11+} were calculated by Teng *et al.* [16] using the configuration-average distorted-wave method. Chen and Reed [17] carried out fully relativistic distorted-wave calculations for the ionization of Kr^{24+} and Kr^{25+}, including contributions from both resonant excitation and excitation-autoionization. Badnell and Pindzola [18] performed level to level distorted-wave calculations for the ionization of Kr^{30+}, Kr^{31+}, and Kr^{32+}, also including contributions from both resonant excitation and excitation-autoionization. Recently, Loch *et al.* [19] reported a complete study of the electron-impact single ionization of the krypton atom and its ions, calculating configuration-average distored-wave cross sections and rate coefficients for all ionization stages.

Partial or relative photoionization cross-section measurements on neutral krypton have been reported [20,21], but neither experimental measurements nor theoretical calculations of absolute photoionization cross sections have been reported for Kr ions. Published electron-impact ionization measurements do not give detailed information on the energy dependence of the cross sections. This paper reports absolute photoionization cross-section measurements for Kr^{5+} in the energy range 74–175 eV and the detailed energy dependence of the cross section for electron-impact ionization of Kr^{5+} in the same energy range.

II. EXPERIMENT

Measurements of photoionization of Kr^{5+} ions were performed using the ion-photon-merged-beams end station lo-

cated at undulator beamline 10.0.1 of the Advanced Light Source (ALS). Since details of the experimental setup and measurement technique have been reported [22], only a brief description is presented here. $^{84}Kr^{5+}$ ions were produced by a compact 10-GHz permanent-magnet electron cyclotron resonance (ECR) ion source and accelerated to an energy of 30 keV. After mass and charge-state selection by a dipole analyzing magnet, the Kr^{5+} ions were collimated and focused by an einzel lens. A series of steering plates positioned and directed the ion beam to a spherical electrostatic deflector which merged it with a photon beam generated by an undulator and monochromatized by a grazing-incidence spherical-grating monochromator. The photoion yield was measured as the photon energy was stepped over the range 74–175 eV. Two-dimensional spatial profiles of the merged ion and photon beams were measured by three translating-slit scanners within the interaction region (length=29.4 cm). A potential of +2 kV was applied to the interaction region to energy-label Kr^{6+} product ions produced therein. A dipole analyzing magnet separated the product ions from the primary Kr^{5+} beam, which was collected in an extended Faraday cup. A spherical electrostatic deflector directed product Kr^{6+} ions onto a stainless-steel plate biased at −550 V, from which secondary electrons were accelerated to a multichannel-plate single-particle detector and counted. Absolute measurements of photoionization cross sections were performed at a number of discrete photon energies. These measurements were used to place the photoion-yield spectrum onto an absolute cross-section scale. The total absolute uncertainty of the photoionization cross-section measurements in this experiment is estimated to be ±23%.

The electron-impact ionization measurement for Kr^{5+} was performed using an electron-ion crossed-beams apparatus at the Multicharged Ion Research Facility at the University of Nevada, Reno. This apparatus has been described in detail previously [23,24]. $^{84}Kr^{5+}$ ions were produced in a 14.4-GHz ECR ion source and accelerated to an energy of 50 keV. After mass and charge-state selection by a dipole analyzing magnet, the Kr^{5+} ions were focused, directed and collimated by einzel lenses, steering plates, and a set of adjustable four-jaw slits. The ion beam was charge-purified by a 90° parallel-plate analyzer and then crossed at right angles by an electron beam generated by an electron gun designed and constructed at Justus-Liebig University (Giessen, Germany) [25]. The Kr^{6+} product ions were separated from the parent Kr^{5+} ion beam by a 90° dipole analyzing magnet. After passing through a 90° electrostatic cylindrical deflector, the product ions were counted by a single-particle detector. The primary Kr^{5+} ion beam was collected by an extended Faraday cup mounted inside the magnet chamber. The electron gun can be moved mechanically, allowing adjustment of the electron beam position to optimize the spatial overlap of the electron and ion beams when the relative cross sections were measured by scanning the electron beam energy. Additionally, this permits a separate measurement of the Kr^{6+} background at a position where there is no overlap of the two beams. The relative cross-section spectrum was obtained by subtracting the uncrossed-beams spectrum from the crossed-beams spectrum. Measurement of the energy dependence of the cross section was made using energy steps as small as 73 meV at optimum beam overlap. The high-statistical-precision spectrum was obtained by scanning over the same electron beam energy range from several tens to hundreds of sweeps, depending on the count rates and signal-to-background ratio.

III. ATOMIC STRUCTURE CALCULATIONS

Theoretical calculations were performed using the Flexible Atomic Code (FAC) [26] and Cowan [27] Hartree-Fock atomic structure code to identify the resonance structures in the measured Kr^{5+} photoionization cross section and to interpret fine details in the electron-impact ionization cross section. Configuration-interaction effects are taken into account by the Cowan code calculation, which is based on *L-S* coupling. The FAC code is fully relativistic based on the Dirac equation, and the fine structure of core-excited autoionizing states that are omitted in *L-S* coupling calculations are treated naturally [28]. The accuracy of calculated resonance energies depends on the size of the basis set. However, even when large basis sets were selected, differences between predicted and measured resonance energy positions were found to be of the order of 1 eV.

In the calculation of $4s \rightarrow np$ excitations, $4s^2 4p$ was selected as the initial configuration and $4s4pnp$ $(6<n<12)$ as the final configuration. For $3d \rightarrow np$ and $3d \rightarrow nf$ core electron excitations, $3d^{10}4s^2 4p$ was chosen as the initial configuration, and $3d^9 4s^2 4pnp$ $(4 \leqslant n \leqslant 9)$, $3d^9 4s^2 4pnf$ $(4 \leqslant n \leqslant 20)$ as the final configurations, respectively. For $4s4p^2 \rightarrow 4s4pnd$ $(n>5)$ and $4s4p^2 \rightarrow 4p^2 np$ $(n>5)$ transitions, the initial configuration $4s4p^2$ and the final configuration $4s4pnd$ and $4p^2 np$ were selected, respectively. To determine the contributions of these states to ionization, the decay rates for these final states were also calculated. The Auger rates were found to be larger than the radiative rates by factors of 100 to 1000. Therefore, absorption oscillator strengths may be easily derived from the measured photoionization resonance strengths.

IV. EXPERIMENTAL RESULTS AND ANALYSIS

A. Photoionization of Kr^{5+}

1. $4s \rightarrow np$ excitatation-autoionizaton

Figure 1 shows the absolute photoionization cross section of Kr^{5+} as a function of photon energy in the range of 74–87.2 eV measured at an energy resolution of 100 meV. The cross section is dominated by resonance structures. The nonresonant direct photoionization cross section is very small in this energy range, consistent with a maximum value of 0.08 Mb estimated using the Cowan code. The electronic configuration of Kr^{5+} is $4s^2 4p$ with the ground state $^2P^0_{1/2}$ and the metastable state $^2P^0_{3/2}$. The ionization potentials tabulated in the National Institute of Standard and Technology (NIST) atomic spectra database [29] for these two states are 78.49 and 77.49 eV, respectively. Resonance structure above the metastable-state threshold is attributed to $4s \rightarrow np$ transitions. It is difficult to assign the individual resonances

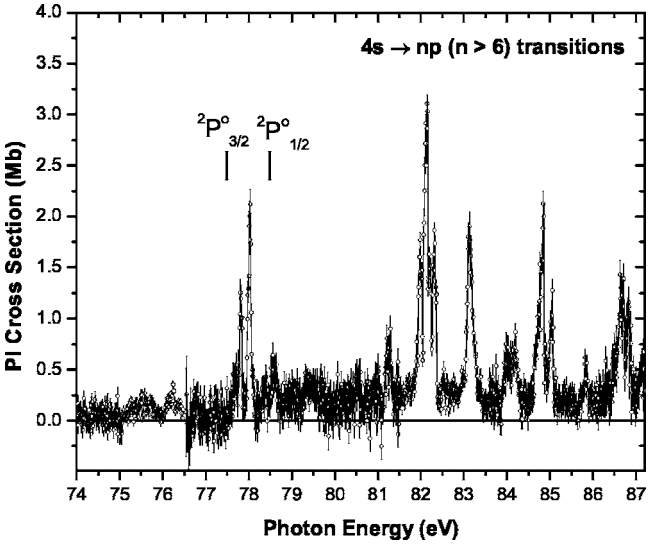

FIG. 1. Absolute photoionization cross section of Kr^{5+} measured with a photon energy resolution of 100 meV, showing $4s \rightarrow np$ transitions. The vertical bars indicate the ionization thresholds for the $^2P^0_{3/2}$ metastable state and the $^2P^0_{1/2}$ ground state.

because there are many transitions in each energy band and the different transition bands overlap.

There are some weak resonances in the energy range between 75 and 76.5 eV, below the threshold of the $4s^24p\ ^2P^o_{3/2}$ metastable state. They could be due to excitation-autoionization from a metastable state of the configuration $4s4p^2\ ^4P$, whose average excitation energy is 13.8 eV above the ground state. The ionization threshold of this state, from which dipole-allowed transitions $4p \rightarrow nd$ and $4s \rightarrow np$ may lead to autoionization, is 64.69 eV. The calculation indicates that the cross section for $4p \rightarrow nd$ transitions from the ^4P metastable state is about 1000 times smaller than that of $4s \rightarrow np$ transitions, whereas the cross section for $4s \rightarrow np$ transitions from this state is comparable to that for $4s \rightarrow np$ transitions from the ground state. In their Kr^{5+} electron-impact ionization measurement, Bannister *et al.* [10] estimated that the fraction in this state was only about 16% of the ion beam produced by the ECR source. Although this metastable fraction was not measured in the present photoionization experiment, energy-scan measurements of electron-impact ionization of Kr^{5+} using an ECR ion source show no evidence of a metastable contribution below 76.5 eV (see Sec. IV B.) Furthermore, the calculation predicts excitations of comparable strength in the energy range 74.0 to 77.5 eV, but there is no evidence of such resonance features in the photoionization measurements. This leads to the conclusion that the fraction of the ion beam in the $4s4p^2$ metastable configuration is negligibly small in both the photoionization and electron-impact ionization measurements reported here. Consequently, the small resonance structures that are observed below 77.49 eV are not due to the excitation of $4s4p^2$ ions in the primary beam.

A previous Xe^{3+} photoionization measurement [30] using the same apparatus and photon beamline indicated the presence of higher-order radiation from the undulator and grating. In that case, significant contamination of the spectrum

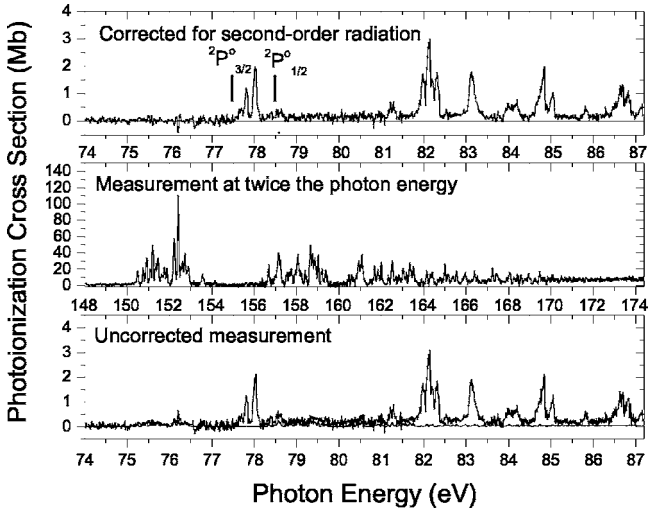

FIG. 2. Corrected near-threshold photoionization cross-section measurement for Kr^{5+} (top panel) shows resonances due to $4s \rightarrow np$ excitation-autoionization. The vertical bars indicate the ionization thresholds for the $^2P^0_{3/2}$ metastable state and the $^2P^0_{1/2}$ ground state. The middle panel shows a measurement made at twice the photon energy, which was scaled to subtract second-order contributions from the raw measurement (bottom panel). Note the large difference in cross-section scales in these two energy ranges.

was produced by features having a large cross section at twice the nominal photon energy. In the present study, features in the range of twice the energy of the $4s \rightarrow np$ spectrum due to $3d \rightarrow np$ $(n > 5)$ and $3d \rightarrow nf$ $(n > 4)$ transitions also have large cross sections, as will be shown later. This second-order contribution was removed from the spectrum of $4s \rightarrow np$ transitions by shifting the $3d \rightarrow np$ and $3d \rightarrow nf$ spectrum into the energy range of this spectrum and subtracting the second-order features point by point. The corrected spectrum is shown in Fig. 2. The vertical lines at 77.49 and 78.49 eV in Fig. 2 mark the ionization thresholds of the $^2P^0_{3/2}$ metastable state and $^2P^0_{1/2}$ ground state, respectively. The corrected cross section below 77.49 eV is zero and is nonzero above this energy. The experimental ionization threshold of the $^2P^0_{3/2}$ metastable state is in agreement with the NIST data. Since the direct nonresonant cross section is very small and there are some resonance structures close to 78.49 eV, the ionization threshold of the $^2P^0_{1/2}$ ground state is not evident from these measurements.

2. $3d \rightarrow 4p$ excitation-autoionization

Figure 3 shows the absolute photoionization cross section of Kr^{5+} as a function of photon energy in the range 87.2–95.1 eV. The photon energy resolution in this measurement was 50 meV. Again, the cross section is dominated by resonance structures. The features in this energy region are attributed to $3d \rightarrow 4p$ transitions. It is difficult to assign the individual resonances because this transition band partly overlaps with the $4s \rightarrow np$ transition band and the fraction of the ion beam in the metastable state is undetermined.

The integrated oscillator strength f for $4s \rightarrow np$ and $3d \rightarrow 4p$ transitions was obtained using the equation [31]

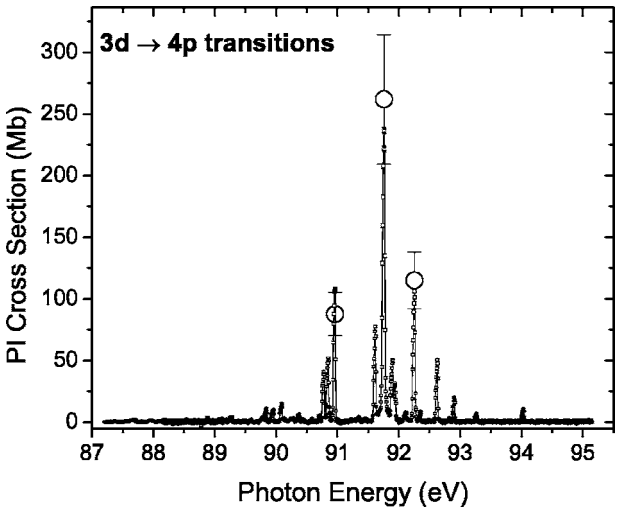

FIG. 3. Absolute photoionization cross section for the $3d \rightarrow 4p$ transition in Kr^{5+} measured with an energy resolution of 50 meV. The large open circles with error bars show absolute cross-section measurements made at the same energy resolution, with their estimated uncertainties.

$$f = (9.11 \times 10^{-3}) \int_{E_1}^{E_2} \sigma(E) dE,$$

where f is dimensionless, $\sigma(E)$ is the cross section in Mb, E is the photon energy in eV, and E_1 and E_2 are the energy limits of the range for which the oscillator strength is to be calculated. The energy interval for the integration is 77.5 to 95.1 eV and the result is presented in the Table I. The calculated oscillator strengths for those transitions using the FAC and Cowan codes, and those for the corresponding transition energy band are also tabulated. For all comparisons between calculations and experiment, a statistical admixture within the ground-state configuration of the $^2P^0{}_{1/2}(1/3)$ and $^2P^0{}_{3/2}(2/3)$ states was assumed to represent the distribution of initial states in the ion beam. For $4s \rightarrow np$ transitions, the oscillator strengths were calculated up to $n=11$.

The difference between the total oscillator strengths obtained from the two theoretical calculations for $4s \rightarrow np$ and $3d \rightarrow 4p$ transitions is about 11%. The differences between these theoretical calculations and the experimental measurement are 23% for the Cowan code and 39% for FAC code. The latter difference exceeds the experimental uncertainty for these transitions. Note that the calculated oscillator strengths for $4s \rightarrow 7p$ transitions are smaller than that for $4s \rightarrow 8p$ transitions in both cases. This is because not all of the $4s \rightarrow 7p$ transitions lie above the ionization threshold.

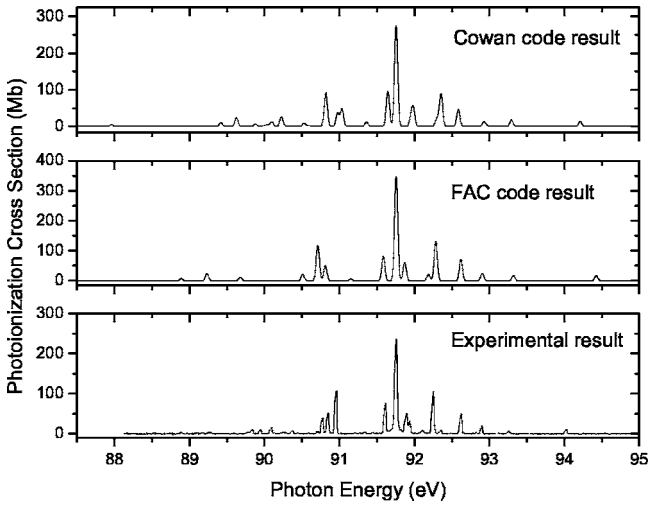

FIG. 4. Comparison of absolute cross-section measurements for photoionization of Kr^{5+} with the theoretical spectra, shifted by +0.90 eV for Cowan code result and by +1.67 eV for FAC code result.

To compare the calculation for $3d \rightarrow 4p$ transitions with experiment, the theoretical spectrum was convoluted with a Gaussian profile accounting for the instrumental function [50 meV full width at half maximum (FWHM)], keeping the total calculated oscillator strength the same before and after the convolution. The results are presented in Fig. 4. The theoretical spectrum is brought into reasonable agreement with the experimental spectrum by shifting the theoretical spectrum by +0.90 eV for the Cowan code result and by +1.67 eV for the FAC code result.

3. $3d \rightarrow np$, nf excitation-autoionization

Figure 5 shows the absolute photoionization cross section for Kr^{5+} in the photon energy range 131.8–175 eV. The pho-

TABLE I. Sum of the oscillator strengths for $4s \rightarrow np$ and $3d \rightarrow 4p$ transitions determined from experiment compared to calculated oscillator strengths for those transitions for $7 \leqslant n \leqslant 11$.

Transition	Oscillator Strengths (Experiment)	Oscillator Strengths (FAC)	Oscillator Strengths (Cowan)	Energy Band (eV) (FAC)	Energy Band (eV) (Cowan)	Energy Range (eV) (Experiment)
$3d \rightarrow 4p$		0.5206	0.4592	85.6–95.0	87.1–95.4	
$4s \rightarrow 7p$		0.0036	0.0038	74.3–83.8	75.4–83.8	
$4s \rightarrow 8p$		0.0082	0.0085	78.6–88.0	79.8–88.0	
$4s \rightarrow 9p$		0.0052	0.0054	81.4–90.7	82.5–90.7	
$4s \rightarrow 10p$		0.0035	0.0036	83.2–92.5	84.4–92.5	
$4s \rightarrow 11p$		0.0025	0.0026	84.5–93.8	85.7–93.8	
Sum	0.391	0.5436	0.4831			77.5–95.1

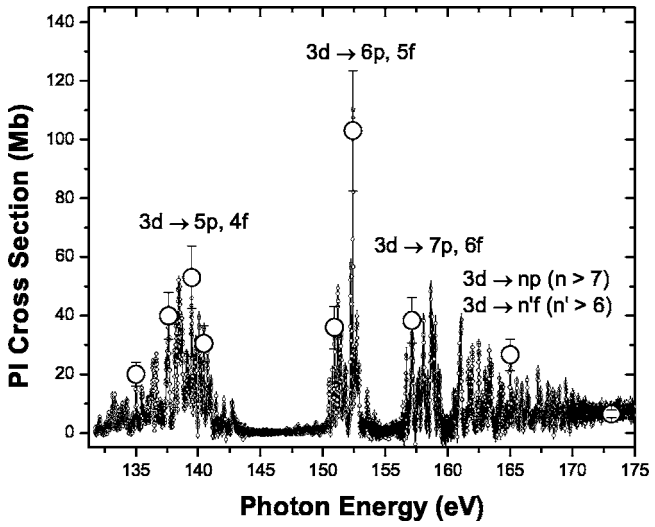

FIG. 5. Photoionization cross section in the energy range of $3d \rightarrow np$ $(n>4)$ and $3d \rightarrow nf$ $(n>3)$ transitions in Kr^{5+} measured with an energy resolution of 100 meV. The large open circles with error bars represent the absolute cross-section measurements and their uncertainties.

ton energy resolution was 100 meV for this measurement. The features in this energy region are attributed to $3d \rightarrow np$ $(n \geqslant 5)$ and $3d \rightarrow nf$ $(n \geqslant 4)$ transitions. It is hard to assign the individual transitions because there are numerous overlapping transition bands, some of which are identified in Fig. 5.

The oscillator strengths and the corresponding energy bands for $3d \rightarrow np$ $(4 \leqslant n \leqslant 9)$ and $3d \rightarrow nf$ $(4 \leqslant n \leqslant 20)$ transitions were calculated using FAC and Cowan codes. The results are presented in Table II along with experimental oscillator strengths and corresponding energy intervals for the integrations. The difference between the total oscillator strengths calculated using the two codes for $3d \rightarrow 5p$ and $3d \rightarrow 4f$ transitions is about 6%. The difference between the experimental measurement and theoretical calculations for the same transitions is about 17% for the FAC code and 22% for the Cowan code. The same comparison for the $3d \rightarrow 7p$ and $3d \rightarrow 6f$ transitions gives 7%, 24%, and 29%. Experiment and theory agree within a few percent for the transitions $3d \rightarrow 6p$ and $3d \rightarrow 5f$.

The total experimental oscillator strength for $3d \rightarrow np$, $nf(n \geqslant 4)$ transitions is 3.30 and the calculated oscillator strengths for the same transitions are 2.8507 for FAC code and 2.6252 for Cowan code. Considering the absolute experimental uncertainty of ±23% and the fact that small parts of the oscillator strengths of the various series are not included, the level of agreement with the theoretical calculations is considered satisfactory.

B. Electron-impact ionization of Kr^{5+}

Electron-impact ionization cross sections of Kr^{5+} are presented in Fig. 6. The electron-energy resolution is approximately 1 eV. The relative yield of Kr^{6+} product ions was measured in a fine energy-scanning mode and normalized to the absolute cross-section measurements of Bannister *et al.* [10] Also shown in Fig. 6 are predictions of the single-parameter Lotz formula [32] for direct single ionization of Kr^{5+},

$$\sigma(E) = 4.5 \times 10^{-14} \sum_j \frac{r_j}{I_j E} \ln(E/I_j),$$

where the cross section σ at a collision energy E (in eV) is given in cm^2, r_j is the number of electrons in subshell j, and I_j is the ionization energy (in eV) for electrons in that subshell. The Lotz formula is both convenient to use and generally gives a reliable prediction for direct ionization. However, it does not include contributions from excitation-autoionization processes. The theoretical direct and total ionization cross sections calculated by Gorczyca *et al.* [14] using configuration-average distorted-wave approximation are also shown in the same figure. The total ionization cross sections were obtained by summing the direct ionization and the excitation-autoionization cross section. The atomic structure of Kr^{5+} is characterized by an Ar core with a $3d^{10}4s^24p$ outer-shell configuration. The calculated configuration-average ionization potentials for these subshells [14] are presented in Table III.

The theoretical direct ionization cross section below 100 eV is in good agreement with the prediction of the Lotz formula, but is a little smaller above this energy. The calculated total ionization cross section and the experimental measurement show the same general behavior throughout the entire energy range. However, the excitation-autoionization cross sections are underestimated by the theoretical calculation below 118 eV. This may be attributed partly to the neglect in the calculation of $4s \rightarrow nl$ excitations, as well as contributions from resonant processes, which are evident in the measurement.

1. $4s \rightarrow nl$ and $3d \rightarrow 4p$ excitation-autoionization

Figure 7(a) shows the electron-impact ionization cross section as function of electron energy for Kr^{5+} in the low-energy region. For comparison, the photoionization measurement in the same energy range is presented in Fig. 7(b). The observed electron-impact ionization threshold near 76.5 eV indicates that the parent Kr^{5+} ion beam contained ions in the $3d^{10}4s^24p\ ^2P^0_{3/2}$ metastable state. Cross section rises more steeply than the Lotz formula prediction from the ionization threshold up to about 94 eV. This suggests a series of excitation-autoionization onsets. Excitation-autoionizations due to $3d \rightarrow 4p$ *and* $4s \rightarrow nl$ $(n>6)$ are likely responsible for most of the enhancement of the cross section over direct ionization. It is noted that $3d \rightarrow 4p$ and $4s \rightarrow np$ $(n>6)$ transitions are apparent in the photoionization cross section in this photon energy range (Figs. 3 and 4). However, apparent enhancement of the electron-impact ionization cross section due to $4s \rightarrow nl$ transitions just above the ionization threshold is significant, whereas the corresponding $4s \rightarrow np$ photoionization cross section is relatively small. A possible explanation is that electric-dipole forbidden transitions that contribute to electron-impact ionization are forbidden in photoionization.

TABLE II. Experimental and calculated oscillator strengths and the corresponding energy intervals for $3d \rightarrow np$ and $3d \rightarrow nf$ transitions.

Transition	Oscillator Strengths (Experiment)	Oscillator Strengths (FAC)	Oscillator Strengths (Cowan)	Energy Band (eV) (FAC)	Energy Band (eV) (Cowan)	Energy Range (eV) (Experiment)
$3d \rightarrow 4p$	0.391[a]	0.5206	0.4592	85.6–95.0	87.1–95.4	87.2–95.1
$3d \rightarrow 5p$		0.0928	0.0753	128.0–135.6	129.7–136.4	
$3d \rightarrow 4f$		0.7463	0.7108	134.1–140.1	135.7–141.2	
Sum	1.01	0.8391	0.7908			131.8–144.1
$3d \rightarrow 6p$		0.0338	0.0292	143.6–149.3	145.7–150.8	
$3d \rightarrow 5f$		0.4723	0.4403	146.0–151.2	148.1–152.8	
Sum	0.502	0.5061	0.4722			147.0–155.0
$3d \rightarrow 7p$		0.0166	0.0147	151.3–156.5	153.5–158.2	
$3d \rightarrow 6f$		0.2885	0.2660	152.6–157.5	154.7–159.2	
Sum	0.399	0.3051	0.2828			156.0–159.5
$3d \rightarrow 8p$		0.0095	0.0085	155.8–160.7	159.9–162.5	
$3d \rightarrow 7f$		0.1849	0.1695	156.5–161.4	158.7–163.1	
Sum		0.1944	0.1780			
$3d \rightarrow 9p$		0.0060	0.0054	158.5–163.4	160.7–165.2	
$3d \rightarrow 8f$		0.1245	0.1137	159.0–163.8	161.2–165.6	
Sum		0.1305	0.1191			
$3d \rightarrow 9f$		0.0876	0.0798	160.7–165.5	162.9–167.3	
$3d \rightarrow 10f$		0.0638	0.0581	161.9–166.7	164.1–168.5	
$3d \rightarrow 11f$		0.0395	0.0436	162.8–167.6	165.0–169.4	
$3d \rightarrow 12f$		0.0368	0.0335	163.5–168.3	165.7–170.1	
$3d \rightarrow 13f$		0.0289	0.0263	164.0–168.8	166.2–170.6	
$3d \rightarrow 14f$		0.0232	0.0210	164.5–169.2	166.7–171.0	
$3d \rightarrow 15f$		0.0188	0.0171	164.8–169.6	167.0–171.4	
$3d \rightarrow 16f$		0.0155	0.0140	165.1–169.8	167.3–171.6	
$3d \rightarrow 17f$		0.0129	0.0117	165.3–170.1	167.5–171.9	
$3d \rightarrow 18f$		0.0108	0.0098	165.5–170.3	167.7–172.1	
$3d \rightarrow 19f$		0.0092	0.0083	165.6–170.4	167.8–172.2	
$3d \rightarrow 20f$		0.0079	0.0072	165.8–170.5	168.0–172.4	
$3d \rightarrow np,nf$ $(n \geqslant 4)$	3.30	2.8507	2.6252	85.6–170.5	87.1–172.4	87.2–173.9

[a]The calculated values in Table I indicate that the oscillator strengths for $4s \rightarrow np$ transitions in this energy range are approximately two orders of magnitude smaller than that for $3d \rightarrow 4p$ transitions.

A comparison of the electron-impact ionization and photoionization cross sections suggests that the change in slope of the former at 91 eV is due to the onset of $3d \rightarrow 4p$ excitation-autoionization.

A feature in the electron-impact cross section near 81.5 eV is below the $3d \rightarrow 4p$ excitation threshold and likely due to the resonant excitation-double-autoionization (REDA) process [33] involving the $3d^9 4s^2 4p^2 nl$ intermediate autoionizing state of Kr^{4+} that decays by sequential ejection of two electrons.

2. 3d→nl excitation-autoionization

Figure 8(a) presents the electron-impact ionization cross section for Kr^{5+} in the energy range 95.5–173.3 eV. For comparison, the photoionization measurement in the same energy range is also shown in Fig. 8(b). The configuration-average excitation and ionization energies of $3d \rightarrow nl$ transitions [14] are also marked by the short vertical lines in Fig. 8(a) and tabulated in Table III. There is some correspondence between the predicted energies and the measured steps.

The $3d \rightarrow np$ $(n \geqslant 5)$ and $3d \rightarrow nf$ $(n \geqslant 4)$ transitions that contribute significantly to the photoionization cross section are not so evident in the electron-impact spectrum. Conversely, the electric-dipole forbidden $3d \rightarrow 4d$ and $3d \rightarrow 5d$ transitions appear to be responsible for the largest features in the electron-impact ionization cross section starting at about 116 eV up to about 131 eV for $3d \rightarrow 4d$ transitions, and at about 142 eV up to about 149 eV for $3d \rightarrow 5d$ transitions. This is consistent with the theoretical prediction by Gorczyca *et al.* [14] that the $3d \rightarrow 4d$ transition contributes a large cross section for electron-impact ionization. The measure-

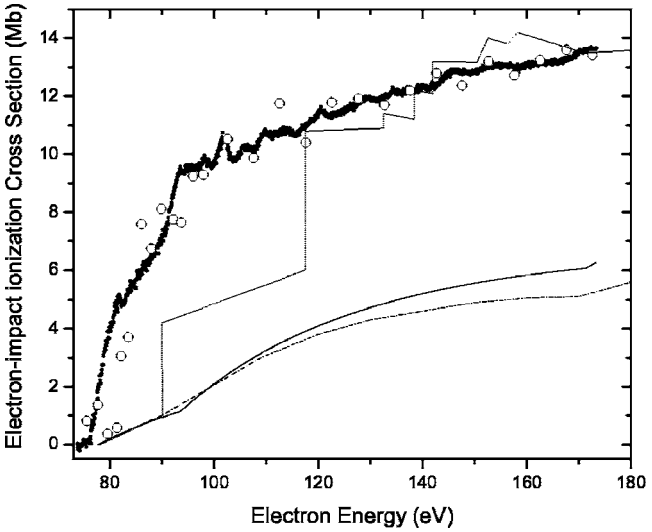

FIG. 6. Energy-scan measurement of the cross section for electron-impact ionization of Kr^{5+} (filled circles) normalized to the absolute measurement of Bannister *et al.* [10] (open circles). The experimental energy resolution is approximately 1 eV. The solid curve is the Lotz formula prediction for the direct ionization cross section. The dot-dashed and dotted curves are direct and total ionization cross sections calculated by Gorczyca *et al.* [14], respectively.

ment additionally suggests that $3d \rightarrow 5d$ and $3d \rightarrow 6d$ transitions also contribute significantly to the electron-impact ionization cross section.

A distinct resonance at 120.5 eV is evident in the electron-impact spectrum. This energy is below the excitation threshold for $3d \rightarrow 5p$ transitions and is most likely due to the REDA process, as discussed above. But one $3d$ inner-shell electron is excited to the $5p$ orbital instead of the $4p$ orbital in this case. Several additional resonance features are evident in the electron-impact ionization cross section between 95.5 eV and the $3d \rightarrow 4d$ excitation threshold. Again, they are attributed to REDA processes involving $3d \rightarrow 4d$

TABLE III. Configuration-average ionization and excitation energies for Kr^{5+} [14]

Subshell	Ionization potential (eV)
$4p$	77.76
$4s$	93.55
$3d$	171.34
Transition	Excitation energy (eV)
$3d \rightarrow 4p$	90.05
$3d \rightarrow 4d$	117.53
$3d \rightarrow 4f$	138.35
$3d \rightarrow 5p$	132.55
$3d \rightarrow 5d$	141.95
$3d \rightarrow 5f$	150.43
$3d \rightarrow 6p$	148.03
$3d \rightarrow 6d$	152.55
$3d \rightarrow 6f$	156.94

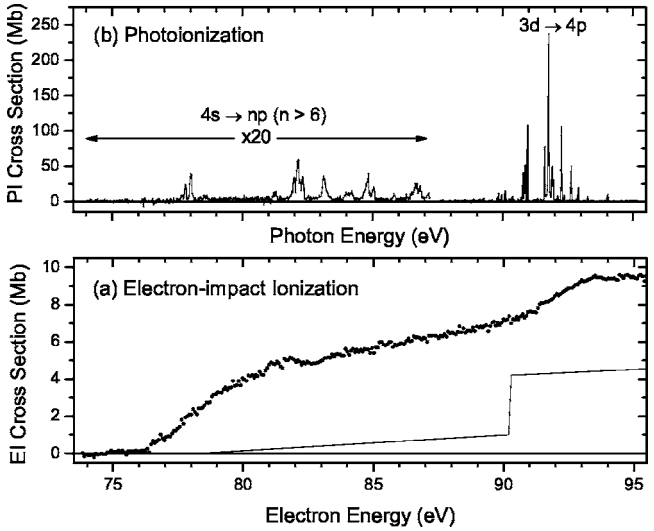

FIG. 7. Comparison of electron-impact ionization cross-section measurements for Kr^{5+} (a) with photoionization cross-section measurements (b) in the energy range 73.8 to 95.5 eV. The photoionization cross section in the energy region from 74 to 87.2 eV has been multiplied by a factor of 20. In (a), the curve is the theoretical ionization cross-section calculation from Ref. [14].

resonant excitation. Finally, a small step in the electron-impact ionization cross section beginning near 170 eV is close to the predicted ionization threshold of the $3d$ subshell. In the energy region between 170 eV and the double ionization threshold of Kr^{5+} at 186 eV, $3d$ ionization leads only to single ionization and likely accounts for the observed step.

V. SUMMARY AND CONCLUSIONS

Absolute cross sections were measured for photoionization of Kr^{5+} in the photon energy range 74 eV–175 eV at

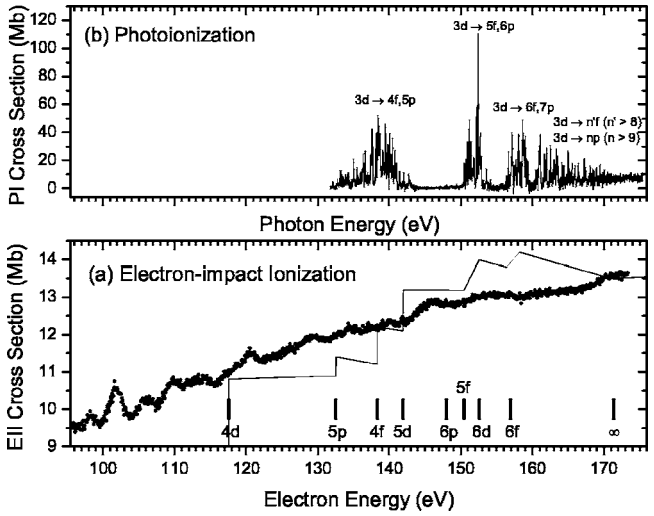

FIG. 8. Comparison of electron-impact ionization cross-section measurement for Kr^{5+} (a) with the photoionization cross section measurement, (b) in the energy range 95.5 to 173.3 eV. In (a), the curve is the theoretical ionization cross section from Ref. [14].

spectral resolutions of 50 meV and 100 meV. The detailed energy dependence of the cross section for electron-impact ionization was also measured in the corresponding range of electron energies.

The FAC and Cowan Hartree-Fock atomic structure codes were used to calculate energy levels, excitation energies, and oscillator strengths for autoionizing transitions from the ground state ($3d^{10}4s^24p\ ^2P^0_{1/2}$) and metastable state ($3d^{10}4s^24p\ ^2P^0_{3/2}$) of Kr^{5+}. The measurements and calculations show that the direct nonresonant photoionization cross section is negligible compared to the resonant contributions to the cross section due to excitation-autoionization processes. The absolute photoionization cross section in the photon energy region 74–87 eV is dominated by excitation of a $4s$ electron into np ($n>6$) orbitals. In the photon energy range of 87–175 eV, the cross section is dominated by excitation of a $3d$ inner-shell electron into np and nf ($n\geqslant 4$) orbitals. The calculations are brought into reasonable agreement with the measurement for $3d\rightarrow 4p$ excitation-autoionization by shifting the theoretical spectrum by +0.90 eV for the Cowan code result and by +1.67 eV for the FAC code result. The measured oscillator strengths are in general agreement with both theoretical calculations within the ±23% experimental uncertainty.

Detailed energy-scan measurements indicate that the electron-impact ionization cross section for Kr^{5+} in the electron energy range 74–87 eV is dominated by $4s$ to nl excitation-autoionization processes. In the electron energy range 95.5–173.3 eV, contributions due to $3d\rightarrow nd$ electric-dipole forbidden transitions dominate the $3d\rightarrow np$ ($n\geqslant 5$) and $3d\rightarrow nf$ ($n\geqslant 4$) electric-dipole allowed transitions. Several resonant excitation-double-autoionization (REDA) features are identified in the electron-impact ionization measurement.

Complementary measurements of photoionization and electron-impact ionization cross sections provide a more detailed basis for understanding the role of autoionization processes in multielectron systems, and would benefit from a more sophisticated theoretical treatment.

ACKNOWLEDGMENTS

The authors are grateful to Bruce Rude for expert technical assistance. This research was supported by the U.S. Department of Energy under Grant No. DE-FG02-03ER15424 and Contract No. DE-AC03-76SF-00098, and by the Deutche Forschungsgemeinschaft under Project No. Mu 1068/10. C.C. acknowledges support from DGAPA-UNAM, México.

[1] K. Widmann, P. Beiersdorfer, V. Decaux, S. R. Elliott, D. Knapp, A. Osterheld, M. Bitter, and A. Smith, Rev. Sci. Instrum. **66**, 761 (1995).
[2] K. W. Hill, S. D. Scott, M. Bell, R. Budny, C. E. Bush, R. E. H. Clark, B. Denne-Hinnov, D. R. Ernst, G. W. Hammett, D. R. Mikkelsen, D. Mueller, J. Ongena, H. K. Park, A. T. Ramsey, E. J. Synakowski, G. Taylor, M. C. Zarnstorff, and the TFTR Group, Phys. Plasmas **6**, 877 (1999).
[3] M. Bitter, H. Hsuan, C. Bush, S. Cohen, C. J. Cummings, B. Grek, K. W. Hill, J. Schivell, M. Zarnstorff, P. Beiersdorfer, A. Osterheld, A. Smith, and B. Fraenkel, Phys. Rev. Lett. **71**, 1007 (1993).
[4] R. Radtke, C. Biedermann, T. Fuchs, G. Fussmann, and P. Beiersdorfer, Phys. Rev. E **61**, 1966 (2000).
[5] H. Chen, P. Beiersdorfer, K. B. Fournier, and E. Träbert, Phys. Rev. E **65**, 056401 (2002).
[6] E. Krishnakumar and S. K. Srivastava, J. Phys. B **21**, 1055 (1988).
[7] J. A. Syage, Phys. Rev. A **46**, 5666 (1992).
[8] B. L. Schram, Physica (Amsterdam) **32**, 197 (1966).
[9] K. Tinschert, A. Müller, G. Hofmann, K. Huber, R. Becker, D. C. Gregory, and E. Salzborn, J. Phys. B **20**, 1121 (1987).
[10] M. E. Bannister, X. Q. Guo, and T. M. Kojima, Phys. Rev. A **49**, 4676 (1994).
[11] M. E. Bannister, D. W. Mueller, L. J. Wang, M. S. Pindzola, D. C. Griffin, and D. C. Gregory, Phys. Rev. A **38**, 38 (1988).
[12] E. M. Oualim, M. Duponchelle, and P. Defrance, Nucl. Instrum. Methods Phys. Res. B **98**, 150 (1995).
[13] M. Khouilid, S. Cherkani-Hassani, S. Rachafi, H. Teng, and P. Defrance, J. Phys. B **34**, 1727 (2001).
[14] T. W. Gorczyca, M. S. Pindzola, N. R. Badnell, and D. C. Griffin, Phys. Rev. A **49**, 4682 (1994).
[15] D. Mitnik, P. Mandelbaum, J. L. Schwob, A. Bar-Shalom, and J. Oreg, Phys. Rev. A **55**, 307 (1997).
[16] H. Teng, P. Defrance, C. Cheg, and Y. Wang, J. Phys. B **33**, 463 (2000).
[17] M. H. Chen and K. J. Reed, Phys. Rev. A **47**, 1874 (1993).
[18] N. R. Badnell and M. S. Pindzola, Phys. Rev. A **47**, 2937 (1993).
[19] S. D. Loch, M. S. Pindzola, C. P. Ballance, D. C. Griffin, D. M. Mitnik, N. R. Badnell, M. G. O'Mullane, H. P. Summers, and A. D. Whiteford, Phys. Rev. A **66**, 052708 (2002).
[20] D. M. P. Holland, K. Codling, J. B. West, and G. V. Marr, J. Phys. B **12**, 2465 (1979).
[21] J. A. de Gouw, J. van Eck, A. Q. Wollrabe, J. van der Weg, and H. G. M. Heideman, J. Phys. B **27**, 3915 (1994).
[22] A. M. Covington, A. Aguilar, I. R. Covington, M. F. Gharaibeh, G. Hinojosa, C. A. Shirley, R. A. Phaneuf, I. Álvarez, C. Cisneros, I. Dominguez-Lopez, M. M. Sant'Anna, A. S. Schlachter, B. M. Mclaughlin, and A. Dalgarno, Phys. Rev. A **66**, 062710 (2002).
[23] R. Rejoub and R. A. Phaneuf, Phys. Rev. A **61**, 032706 (2000).
[24] M. Lu and R. A. Phaneuf, Phys. Rev. A **66**, 012706 (2002).
[25] M. Stenke, K. Aichele, D. Hathiramani, G. Hofmann, M. Steidl, R. Völpel, and E. Salzborn, Nucl. Instrum. Methods Phys. Res. B **98**, 573 (1995).
[26] Ming Feng Gu, *Atomic Processes in Plasmas*, edited by J. S. Cohen, S. Mazevet, and D. P. Kilcrease, AIP Conf. Proc. No. 730 (AIP, New York, 2004), p. 127; URL: http://kipac-tree.stanford.edu/fac/

[27] R. D. Cowan, *The Theory of Atomic Structure and Spectra* (University of California Press, Berkeley, 1981).
[28] M. F. Gu, Astrophys. J. **590**, 113 (2003).
[29] Yu. Ralchenko, A. E. Kramida, J. Reader, A. E. Kramida, W. C. Martin, A. Musgrove, E. B. Saloman, C. J. Sansonetti, J. Reader, and J. J. Curry, http://physics.nist.gov/cgi-bin/AtData/main_asd
[30] E. D. Emmons, A. Aguilar, M. F. Gharaibeh, S. W. J. Scully, R. A. Phaneuf, A. L. D. Kilcoyne, A. S. Schlachter, I. Álvarez, C. Cisneros, and G. Hinojosa, Phys. Rev. A **71**, 042704 (2005).
[31] H. Kjeldsen, P. Andersen, F. Folkmann, J. Hansen, M. Kitajima, and T. Andersen, J. Phys. B **35**, 2845 (2002).
[32] W. Lotz, Z. Phys. **216**, 241 (1968).
[33] G. Hofmann, A. Müller, K. Tinschert, and E. Salzborn, Z. Phys. D: At., Mol. Clusters **16**, 113 (1990).